Robust attitude control of a telescope with flexible modes

D. Alazard[a], J.P. Chrtien[a] & M. Le Du[b]
[a] *CERT-ONERA, 2, Avenue E. Belin, 31400 Toulouse, France*
[b] *CNES, 18, Avenue E. Belin, 31400 Toulouse, France*

Abstract

The requirements concerning satellite optical instruments pointing stability are getting more and more stringent. To put up with a disturbed dynamic environment, the Line-of-Sight (LOS) control laws have to be efficient over a large bandwidth. One of the main performance limitation comes from the flexible modes of these optical payloads and their variations w.r.t host satellite configuration. To solve this problem, both classical frequency domain and modern H_2/H_∞ syntheses have been performed and validated on the CAT experimental test facility (CAT: Contrôle d'Attitude de Télescope).

1 Introduction

As the on-board optical payloads will require higher accuracy, solutions to provide Line Of Sight (LOS) stabilization in a severe dynamic environment consist mainly in rejection of the supporting base disturbances and the problem can be simplified in the following alternative: coupled or decoupled control architecture. CNES (the French Space Agency) conducts both analytical and experimental studies on this subject in order to optimize the design through these two approaches in analyzing the dynamic interaction between the payload and the spacecraft. Two kinds of control architectures have been studied to perform LOS stability :

- dynamic isolation using encoders and accelerometers in order to decrease the natural coupling provided by a soft mounted system,
- disturbance rejection using an inertial reference through an optical reference sensor in order to control the micro-vibrations.

An optimal solution can be achieved in mixing isolation and rejection. However a major limitation comes from the flexible modes of the payload.

This paper will present the analyses that have been performed by CERT-ONERA/DERA under CNES contract to carry out this problem in order to provide both performance and robustness. In the second section, a short description of the experimental test facility (CAT) is proposed. The dynamic modeling of the mock-up, the sensors and the various perturbations acting on the system are presented in the third section. The fourth and the fifth ones are respectively dedicated to the presentation of a classical frequency solution and a modern H_2/H_∞ solution to the disturbance rejection problem. The first one is based on the control of the phase shift of the main resonances. The second one is derived from a pure performance standard form which has been completed by a block expressing insensitivity to the flexible modes. Both solutions are compared and validated on the experimental breadboard.

2 Test facility description

The experimental mock-up is composed of a two axis gimbal system mounted on Bendix flexural pivots (see Figure 1). The "inertial" line of sight of the telescope is simulated with an incoming laser beam reflected on CAT mirror towards a CCD matrix which provides the position. With a smaller field of View, a PSD (Position Sensitive Detector) sensor measures the LOS jitter (not used as a feedback sensor) with an accuracy better than 1 microradian.

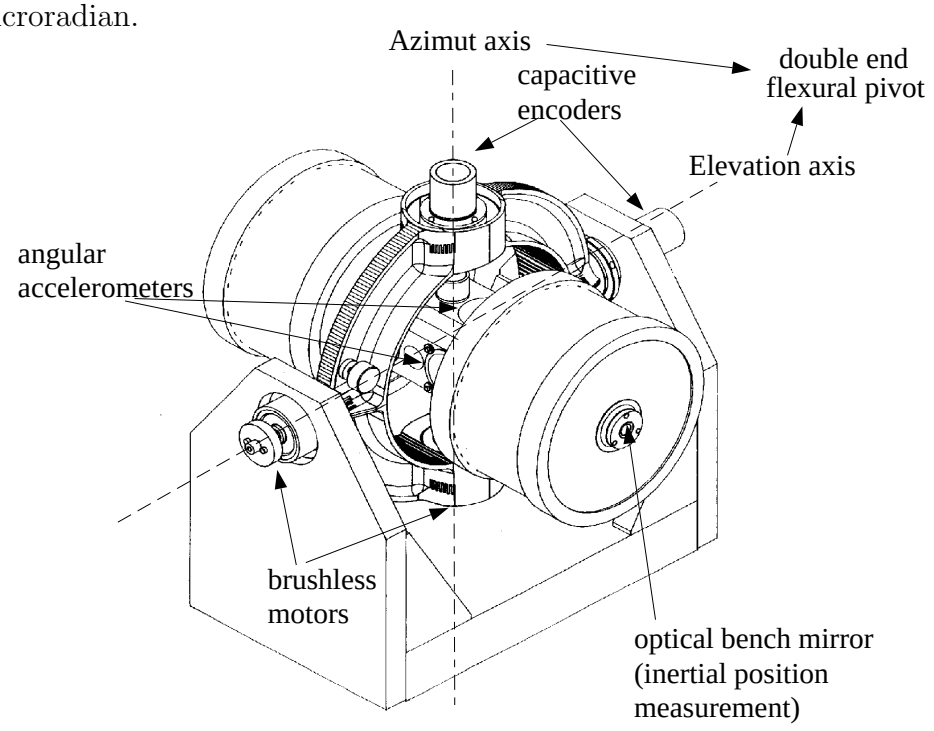

Figure 1: CAT laboratory breadboard

3 Open loop modeling

The specific features of this multi-body system are the small angular range and the absence of friction in joints because of the flexible bearings. So, the linearity assumption is quite sufficient and realistic for this system. Then, the dynamic behavior of the telescope mounted on Bendix pivots can be represented by the feedback form shown on Figure 2.

This representation includes, in a generalized TITO (Two Input/Two Output) form :

- disturbances from the satellite : θ_s and $\dot{\theta}_s$,
- control variable (torque): u,
- controlled outputs : θ_p and $\dot{\theta}_p$,
- measurements : $\ddot{\theta}_p^m$, θ_r^m and θ_p^m.

This form, also called standard form in the modern synthesis framework, is well adapted to describe our problem and it shows clearly the inputs and the outputs of the controller $K(Z)$ which must be designed in order to minimize the disturbance rejection function $\theta_p/\theta_s(s)$ (expressed as a H_2 or H_∞ norm), i.e. the transfer between the perturbations (position and velocity of the host vehicle) and the controlled outputs (position and velocity of the telescope).

The main dynamic parameters which govern the rigid behavior of the telescope are displayed in Table 1. In fact, the telescope inertia cannot be reduced to its steady state gain and the notation $1/I(s)$ in Figure 2 represents the identified transfer matrix between the two accelerations measured on the telescope main body and the two torques applied on the joints (non-collocated transfer). The frequency response of this 40th order identified model is displayed on Figure 7: a certain number of modes are located between 600 and $1600\,rd/s$. As we will see in the next sections, these flexible modes will be driving factors for the control law synthesis.

To conclude with the dynamic modeling of the mock-up, we want to highlight the following points which will steer the following developments:

- the sample rate ($500\,Hz$) is close to the highest frequency of the flexible modes, so the synthesis must be led in discrete time domain in order to take into account the phase shift brought in by the zero order hold and the sampling,
- the inertial telescope position and acceleration measurements are perturbed respectively by a large pure delay ($\tau = 0.06\ s$) due to the CCD camera matrix updating (modeled by a first order Pad approximation on Figure 2) and a bias ($\ddot{\theta}_0$) which is unknown and may change with thermal variations.

	elevation	azimuth
Rigid inertia : $I = I(s)_{\|s=0}$	0.46 $(Kg\,m^2)$	0.35 $(Kg\,m^2)$
Bendix stiffness : k_B	0.44 (Nm/rd)	1.136 (Nm/rd)
Bendix damping : f_B	0.15 (Nms/rd)	0.046 (Nms/rd)
Pure delay : τ	0.06 s	0.06 s
Accelerometers : $\frac{\omega_1^2}{s^2+\sqrt{2}\omega_1 s+\omega_1^2}$	$\omega_1 = 2\pi 198\, rd/s$	$\omega_1 = 2\pi 202\, rd/s$
Anti-aliasing filters : $\frac{\omega_2^2}{s^2+\sqrt{2}\omega_2 s+\omega_2^2}$	$\omega_2 = 2\pi 100\, rd/s$	$\omega_2 = 2\pi 100\, rd/s$
Encoders : $\frac{\omega_3}{s+\omega_3}$	$\omega_3 = 2\pi 10\, rd/s$	$\omega_3 = 2\pi 10\, rd/s$

Table 1: Main dynamic parameters

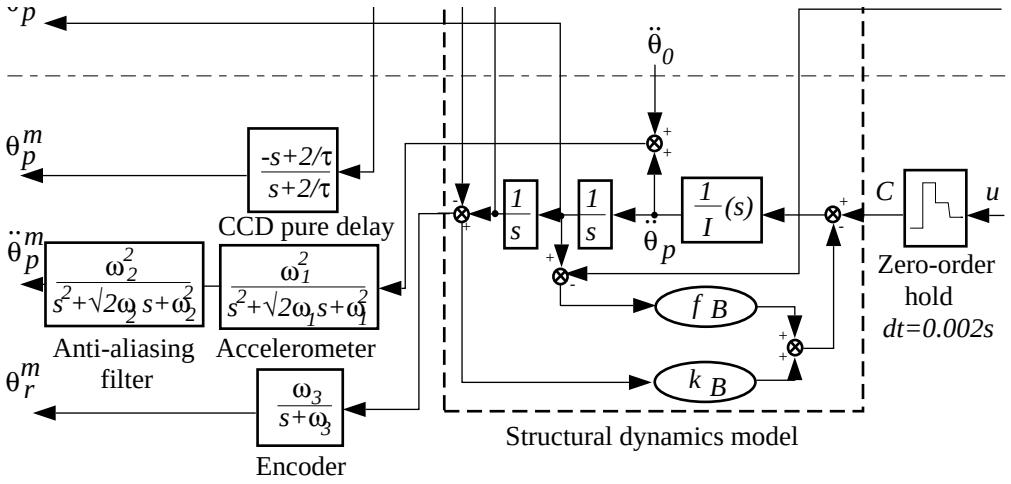

Figure 2: Open loop model $G(Z)$

Notations:

- θ_p : inertial angular position of telescope (rd)
- $\dot{\theta}_p$: inertial angular velocity of telescope (rd/s)
- $\ddot{\theta}_p$: inertial angular acceleration of telescope (rd/s^2)
- θ_s : inertial angular position of host satellite (rd)
- $\dot{\theta}_s$: inertial angular velocity of host satellite (rd/s)
- θ_r : relative angular position of telescope w.r.t satellite (rd)
- C : joint input torque (Nm)
- u : digital control variable (Nm)
- e or a : subscripts standing for "elevation" and "azimuth" axes
- m : superscript standing for "measurement"

4 Classical frequency domain synthesis

4.1 Rigid case

By "rigid case", we mean that the telescope is considered rigid, i.e. that the dynamic inertia $I(s)$ is reduced to its steady state gain I; flexible bearings are however still considered. Therefore the open loop rejection function reads:

$$\frac{\theta_p}{\theta_s}(s) = \frac{f_B s + k_B}{I s^2 + f_B s + k_B} \tag{1}$$

A simple and efficient control law consists of a classical proportional-derivative control on θ_p^m (see gains K_p and K_v on Figure 4) to provide low frequency rejection by the mean of an inertial position servo-loop. This control is then completed by an acceleration feedback (through a gain K_a shown on Figure 4) in order to increase the apparent inertia and to provide thus high frequency rejection. The relative position (θ_r^m) is not used because a feedback on this measurement would create couplings between the host vehicle and the telescope motions and so may affect the disturbance rejection function. If parasitic sensor dynamics are neglected, then the closed-loop rejection function reads:

$$\frac{\theta_p}{\theta_s}(s) = \frac{f_B s + k_B}{(I + K_a) s^2 + (f_B + K_v) s + k_B + K_p} \tag{2}$$

From a practical point of view, the tuning of these three gains is limited by the phase lag introduced by sensors dynamics (accelerometers, anti-aliasing filters, pure delay on inertial position measurement,...):

- tuning acceleration loops to a $3\,dB$ gain margin leads to $K_a = 0.65$ and $0.5\,kg\,m^2$ respectively on elevation and azimuth axis. These values are mostly depending upon the analog anti-aliasing filter frequency and can not be improved without hardware modifications,
- K_p and K_v are strongly limited by pure delay ($\tau = 0.06\,s$ leads to a $180°$ phase lag at $50\,rd/s$) and by accelerometer bias $\ddot{\theta}_0$ which does not allow direct estimation of inertial velocity from acceleration integration.

The tuning of these last two gains can be improved if we consider that the two kinds of inertial sensors (CCD camera and accelerometer) give complementary measurements in frequency domain. So, a Kalman filter has been designed on each axis to estimate the three inertial states (position, velocity and acceleration) from both measurements (see Figure 4).

The Kalman model displayed on Figure 3 takes into account the two integrations between acceleration and position, the pure delay τ and the acceleration bias $\ddot{\theta}_0$ and leads to the fourth order state space representation:

$$\begin{bmatrix} \dot{x} \\ \theta_p \\ \dot{\theta}_p \\ \ddot{\theta}_0 \end{bmatrix} = \begin{bmatrix} -2/\tau & 4/\tau & 0 & 0 \\ 0 & 0 & 1 & 0 \\ 0 & 0 & 0 & -1 \\ 0 & 0 & 0 & 0 \end{bmatrix} \begin{bmatrix} x \\ \theta_p \\ \dot{\theta}_p \\ \ddot{\theta}_0 \end{bmatrix} + \begin{bmatrix} 0 \\ 0 \\ 1 \\ 0 \end{bmatrix} \ddot{\theta}_p^m \qquad (3)$$

$$\theta_p^m = \begin{bmatrix} 1 & -1 & 0 & 0 \end{bmatrix} \begin{bmatrix} x & \theta_p & \dot{\theta}_p & \ddot{\theta}_0 \end{bmatrix}^t$$

As the pure delay is well known, only the two measurements and the bias are perturbed. So, according to Figure 3, the state and output noise covariance matrices have been tuned in the following way :

$$Q = \begin{bmatrix} 0 & 0 & 0 & 0 \\ 0 & 0 & 0 & 0 \\ 0 & 0 & 1 & 0 \\ 0 & 0 & 0 & 10000 \end{bmatrix} \quad \text{and R} = 1 \qquad (4)$$

The three estimated inertial states are readily deduced from the state estimates and the measurements:

$$\begin{bmatrix} \widehat{\theta_p} \\ \dot{\theta}_p \\ \ddot{\theta}_p \end{bmatrix} = \begin{bmatrix} 0 & 1 & 0 & 0 \\ 0 & 0 & 1 & 0 \\ 0 & 0 & 0 & -1 \end{bmatrix} \begin{bmatrix} \widehat{x} \\ \theta_p \\ \dot{\theta}_p \\ \ddot{\theta}_0 \end{bmatrix} + \begin{bmatrix} 0 & 0 \\ 0 & 0 \\ 0 & 1 \end{bmatrix} \begin{bmatrix} \theta_p^m \\ \ddot{\theta}_p^m \end{bmatrix} \qquad (5)$$

This Kalman filter is then discretized by the Tustin transformation and implemented on each mono-axis loop according to Figure 4. It allows to reach the proportional-derivative tuning displayed on Table 2. This tuning is quite efficient and yields a $75\,dB$ attenuation up to $100\,rd/s$ on both axes (the rejection function achieved in the rigid case can be illustrated by the low frequency responses ($\omega < 500\,rd/s$) of Figure 11).

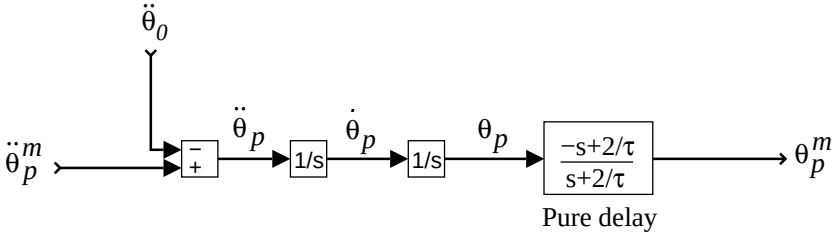

Figure 3: Kalman model for inertial state estimation

4.2 Flexible case

Now, let us consider the flexible modes of the telescope. In order to reduce the order of the two mono-axis synthesis models, the 40th order identified model ($1/I(s)$) has been truncated in the balanced representation to

14th and 10th orders for elevation and azimuth axis respectively (see Figure 7). The full order model is only used for validation in the MIMO case (2 axes with couplings) and for comparison with experimental results (Figure 11.b).

Figure 8 is a drawing of the open-loop Nichols plot ($K(Z)G(Z)$) for elevation axis and shows clearly that several flexible modes become unstable with the rigid control (i.e. control synthesized under rigid assumption).

We want to emphasize the elevation axis case because, from a model reduction point of view, control synthesis is conditioned by only three flexible modes:

- the mode at $1160\,rd/s$ because it provides the greatest resonance,
- the first two flexible modes (650 and $800\,rd/s$) because there is no flexible zeros between these two modes and so there is a 180° phase lag between two resonances.

From the model reduction point of view, there is however no usual reduction method which leads readily to a reduced model with and only with these three modes. Using the balanced approach, order 14 (i.e. 7 modes) corresponds to the minimum value to retain these modes in the elevation synthesis model.

In order to stabilize the elevation axis, there was no way to find a low-pass filter selective enough to bring these resonances under the $0\,dB$ axis on Nichols plots without low frequency performance degradation. Too selective notch filters (i.e. pole/zero quasi-cancellations) must be avoided because the resonance frequencies are subject to variations according to the host satellite configuration.

An alternative solution to gain control consists of a filter with a non-minimum phase zero between the first two flexible modes (see Figure 10), in order to provide a large phase lag between these two frequencies. The filter is also chosen in order to place the main resonance ($1160\,rd/s$) between two critical points on the Nichols plot. Lastly, this filter must have a low pass behavior to cut off high frequency resonances and prevent spill-over.

This technique, called also phase control of the flexible modes, has been applied on both axes. The designed structural filters are displayed on Table 2 and are introduced in the loop according to Figure 4.

Figures 9 and 10 show respectively the new open-loop Nichols plot and root locus for elevation axis. On the first one, we can see that main resonances are located as far as possible from critical points and the $3\,dB$ gain margin is restored. On the second one, we can see that the loop gain is limited in middle frequency (in fact, this limitation, around $250\,rd/s$, is due to the anti-aliasing filter frequency as in the rigid case) and the most resonant flexible mode at $1160\,rd/s$ is damped in a significant way.

It can be noticed that the two-axis final control law is a 14th order discrete controller. This controller has been implemented on the test facility: experimental open loop and closed loop rejection functions (elevation axis) are displayed on Figure 12. Closed loop behavior is quite satisfying with a rejection rate under $-75\,dB$ for all frequencies. One can compare these results with those predicted by analysis from the full order identified model (Figure 11), especially at high frequencies: the damping improvement of the main resonance ($-15\,dB$ at $1160\,rd/s$ on Figure 11.b) achieved in closed loop is quite similar on both responses.

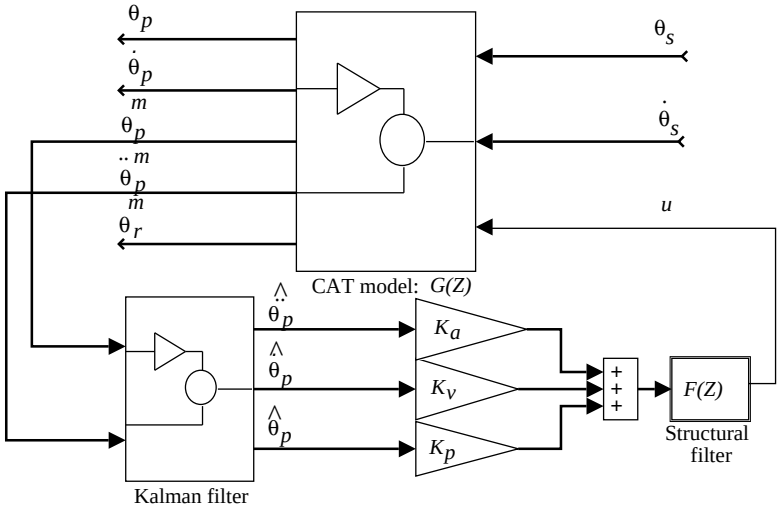

Figure 4: Classical frequency domain solution

	elevation	azimuth
$F(Z)$	$\frac{0.116Z^2-0.044Z+0.142}{Z^2-1.075Z+0.289}$	$\frac{1}{Z}\,\frac{0.5Z^2-0.6Z+0.26}{Z^2-1.2Z+0.36}\,\frac{Z+1}{2Z}$
$K_a\ (Kg\,m^2)$	0.65	0.5
$K_v\ (Nms/rd)$	90	70
$K_p\ (Nm/rd)$	4000	3500

Table 2: Classical control tuning

5 H_2/H_∞ synthesis

The synthesis of a structural filter like $F(Z)$ in frequency domain presented in the previous section requires a long trial and error procedure in the development of the control law. In the present section, we will try to put the disturbance rejection problem in the standard form to apply H_2/H_∞ synthesis and to set up a systematic synthesis procedure. From a methodological point of view, the challenge is to highlight, in this standard

form, the parameters which control the trade-off between performance and robustness w.r.t parametric variations of the flexible modes.

In order to decrease the controller order, we have taken into account the results of the previous frequency domain analysis and reduced the dynamic model ($1/I(s)$ in Figure 2) to the 6th order by visual selection (3 flexible modes: 650, 800 and $1200\,rd/s$; see Figure 7). Finally, the H_2/H_∞ synthesis model (called Gr on Figures 5 and 6) is transformed from discrete to continuous domain by inverse Tustin transformation. In this manner, we can use classical analysis and synthesis toolboxes which are more efficient and more powerful in continuous domain. Final validations will be performed with the discrete controller derived from continuous synthesis results by direct Tustin transformation, applied to the discrete model built from 14th order inertia model (i.e. the model used to build up the classical synthesis).

5.1 Pure performance H_2 synthesis

The pure performance standard form is readily obtained by regularization of the natural form displayed on Figure 2, which cannot be used as it is singular w.r.t. optimization algorithms. This regularization requires :

- 3 extra disturbing inputs (number 1, 2 and 3 on Figures 5 and 6) acting as measurement noises and involving 3 static weightings (w_1, w_2 and w_3) and a low frequency weighting function to specify that acceleration bias must be washed out by the control law,
- 1 extra controlled output (number 1 on figures 5 and 6) to weight the control in the equivalent LQ criterion with a gain r.

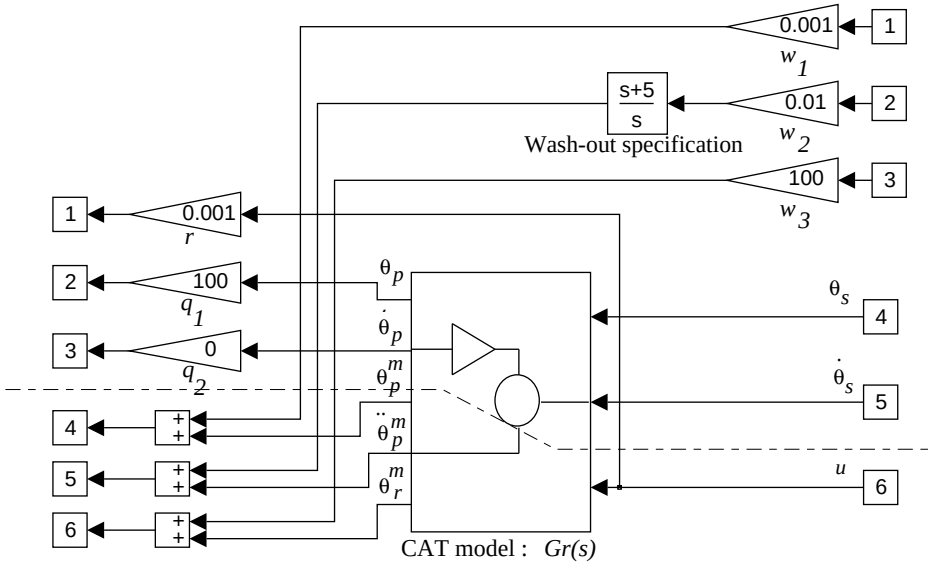

Figure 5: Standard form for pure performance synthesis

Weighting parameters have been tuned by a LQG-like approach and H_2 synthesis using this form leads to a closed loop rigid behavior comparable with the result obtained previously by classical approach, from both bandwidth and rejection rate points of view.

Now, a closer look to the flexible modes (Figure 14) shows that H_2 controller pole/zero pairs cancel the first two flexible pole/zero pairs of the system (650 et $800\,rd/s$). The robustness of such a solution is very marginal and the validation presented on Figure 15 with a more complete model disqualifies this synthesis.

5.2 Robust H_2/H_∞ synthesis

The previous standard form has been therefore completed to take into account robustness constraints.

First, a high pass filter has been introduced in the control weighting function to specify a high frequency roll off behavior for the control law. So the filter zero ($200\,rd/s$) has been tuned just over the desired bandwidth ($100\,rd/s$). In this way, the solution will be insensitive to unmodeled flexible modes (spillover), but this is not efficient to inhibit pole/zero cancellations around the low frequency flexible modes introduced into the synthesis model.

Then, each of these three flexible modes have been perturbed by an additional disturbing noise to provide insensitivity to flexible modes variations. These extra inputs can also be considered as a modelling of a parametric variation of the flexible modes relative damping ratio ξ. Let us consider the i^{th} flexible mode of the structural model $\frac{\ddot{\theta}_p}{C}(s) = \frac{1}{I}(s)$ in a vertical companion state-space form; let ω_i be the natural pulsation of this i^{th} flexible mode and $[q_i^1, q_i^2]$ be the associated elementary state vector. Now consider a fictitious input e_i acting only on the first state variable q_i^1 with a gain ω_i, the state representation reduced to the i^{th} flexible mode reads:

$$\begin{aligned} \begin{bmatrix} \dot{q}_i^1 \\ q_i^2 \end{bmatrix} &= \begin{bmatrix} -2\xi\omega_i & 1 \\ -\omega_i^2 & 0 \end{bmatrix} \begin{bmatrix} q_i^1 \\ q_i^2 \end{bmatrix} + \begin{bmatrix} \alpha_i \\ \beta_i \end{bmatrix} C + \begin{bmatrix} \omega_i \\ 0 \end{bmatrix} e_i \qquad (6) \\ \ddot{\theta}_p &= \begin{bmatrix} c_i & 0 \end{bmatrix} \begin{bmatrix} q_i^1 \\ q_i^2 \end{bmatrix} \end{aligned}$$

and a feedback between output $\ddot{\theta}_p$ and input e_i expresses a variation on the damping ratio ξ.

It can be shown (cf. [1]) that LQG (H_2) synthesis exhibits asymptotic robustness properties to the variations of this parameter if the state noise covariance matrix is chosen in the fictitious input direction for the Kalman filter computation. So, the three additional inputs (number 6, 7 and 8 on

Figure 6) correspond to the three fictitious inputs (e_i, $i = 1, 2, 3$) associated to the three flexible modes. In order to harmonize the variation magnitude between the various modes, we have chosen $\|c_i\| = 1$ (this choice is always possible in MIMO case, c_i being a column vector).

H_2 and H_∞ syntheses have been performed on the final form presented on Figure 6. Validation results are displayed on Figures 16 and 17. The following points are worth to be mentioned:

- H_2 and H_∞ syntheses provide the same solution. It is well-known that H_2 solution is a γ-suboptimal solution of H_∞ problem, but in our particular practical case, the problem is expressed and constrained in such a way that the "distance" between H_2 and H_∞ solution is very small (relative tolerance in γ-iteration was 0.001 and optimal value was $\gamma_{opt} = 21.111$),

- the solution is quite robust with better gain and phase margins than those achieved using the classical approach. We can see on the root locus that controller singularities are far away from plant singularities. This decoupling between controller and plant dynamics depends readily upon the common tuning parameter ($K = 5$ on Figure 6) and guarantees insensitivity to flexible modes. This root locus, by comparison with Figure 10, reveals a non-minimum phase zero between the first two flexible modes, so that synthesis using the standard form is shown to provide phase control in a systematic manner.

Finally, this procedure has been validated on the azimuth axis model and on a 32th order two-axis model. The final multivariable controller has been reduced to 22th order using the balanced approach without any robustness or performance degradation and implemented on the experimental mock-up. Notice that the order of this solution is not so large w.r.t the classical approach one (14th order). Experimental results are displayed on Figure 13: they confirm good performances, comparable with those achieved using a classical approach. The resonance at $200\,rd/s$ visible on Figures 11.a and 12.a has vanished on Figure 13.a : this is the result of phase and gain margins improvements around the first critical point (cf. Nichols plots on Figures 9 and 16).

Figure 13.b allows to compare the LOS rejection functions measured at two different locations on the telescope: one is collocated with the accelerometer (the response is the acceleration twice integrated), and one with the mirror (the response is the PSD measurement), see Figure 1 for physical interpretation. The difference between these responses gives an idea of the mechanical impedance between these two points, which had not been identified. From a practical point view, the last plot (PSD) defines the rejection rate of the control law and it is thus clear that the non-collocation between accelerometers and real LOS can reduce achievable

closed loop performance. From the control law point of view, it should be interesting to evaluate syntheses taking into account the motion at the mirror location in the standard form, either using the PSD measurement or an impedance model of the telescope.

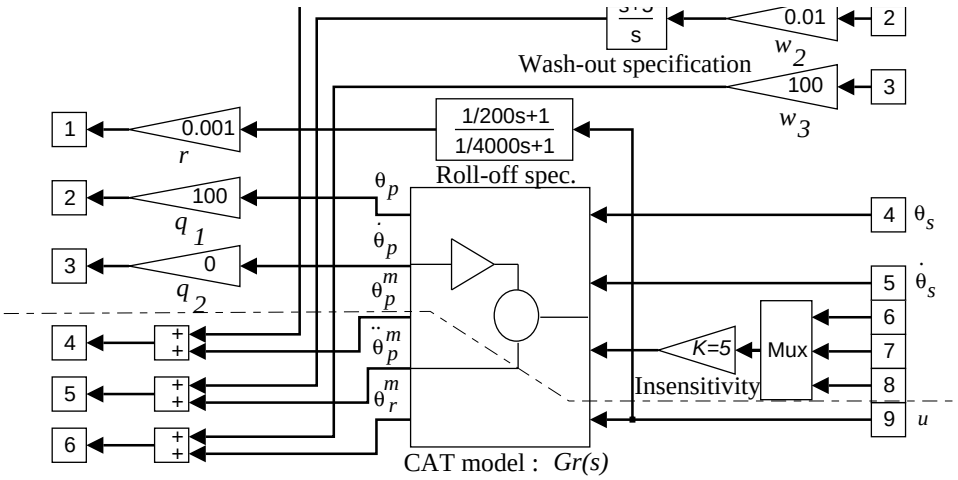

Figure 6: Standard form for robust synthesis

6 Conclusions

Both classical frequency domain and modern H_2/H_∞ syntheses have been compared and validated on the CAT facility. Experimental results demonstrate that complementary sensors (inertial acceleration and position measurements) allow to perform very efficient control laws to reject the host satellite disturbances ($-75\,dB$ up to $100\,rd/s$). The classical approach involves a 4th order Kalman filter on each axis to estimate the inertial states on a wide frequency range and a structural filter to control the flexible modes of the telescope. Modern robust control framework allows us to embed these functions in the standard form and control the performance/robustness trade-off.

Further investigations will be led in three directions:

- from the model reduction point of view, it would be very interesting to establish a systematic and straightforward procedure retaining the sole flexible modes which are driving factors for the control law synthesis (3 modes for the elevation axis case for example), without a visual inspection of the frequency responses: such a reduction method must take into account some robust control considerations in its selection index,

- from the robust control point of view, further studies will be performed in order to extend the methodological approach, demonstrated here on the basis of an identified model, to the case where an analytical model only is available; the relevance of such a model is the possibility to deal with changes of impedance of the supporting structure, and to isolate the parameters which could represent the effect of these changes: the synthesis could then take into account some variations on these parameters to guarantee robustness w.r.t various host satellite configurations,
- from the experimental point of view, the next validation phase will consist in a change of the support of CAT, and to place it on a vibrating table: the experimental illustration of a realistic rejection of host disturbing motions and of robustness of the control w.r.t support changes will be possible.

References

1. Lane Dailey, R. Lecture notes for the workshop : H_∞ and μ methods for robust control, *American Control Conference*, San Diego, California, May 21-22 1990.
2. Tahk, M. & Speyer, J.L. Modeling of parameter variations and asymptotic LQG synthesis, pp. 1-3 to 1-26, *IEEE Transactions on automatic control*, September 1987, **5**(9).
3. Maciejowski, J.M. *Multivariable feedback design.* Electronic systems engineering series. Addison-Wesley, 1989.
4. Kwakernaak, H. & Sivan, R. *Linear optimal control systems.* Wiley interscience. John Wiley and Sons, 1972.
5. Oustaloup, A., editor *La robustesse. Analyse et synthèse de commandes robustes.* Trait des nouvelles technologies, srie Automatique. Herms, 1994.
6. Sefton, J. & Glover, K. Pole/zero cancellations in the general H_∞ problem with reference to a two bloc design. *Systems and Control Letters*, 1990, **14**, pages 295-306.
7. Le Du, M. Optical pointing stability achievement through isolation. *SPIE Proceedings*, 1995.
8. Alazard, D. & Chrétien, J.P. *Commande d'attitude de télescope robuste aux flexibilités de structures.* Rapports Techniques 1 et 2/7950, CNES/DERA, Janvier et Mai 1995.
9. Apkarian, P., Chrétien, J.P. & Biannic, J.M. *Robustesse paramétrique de la commande des systèmes polyarticulés flexibles.* Rapport final 2/7818, DRET/DERA, Avril 1993.

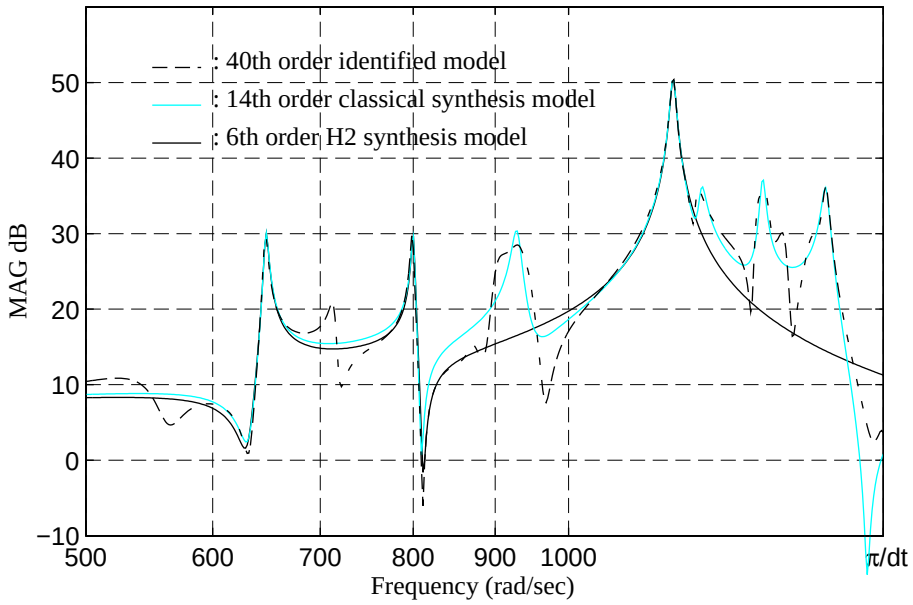

Figure 7: Structural dynamics models $(1/I(s))$ (elevation axis)

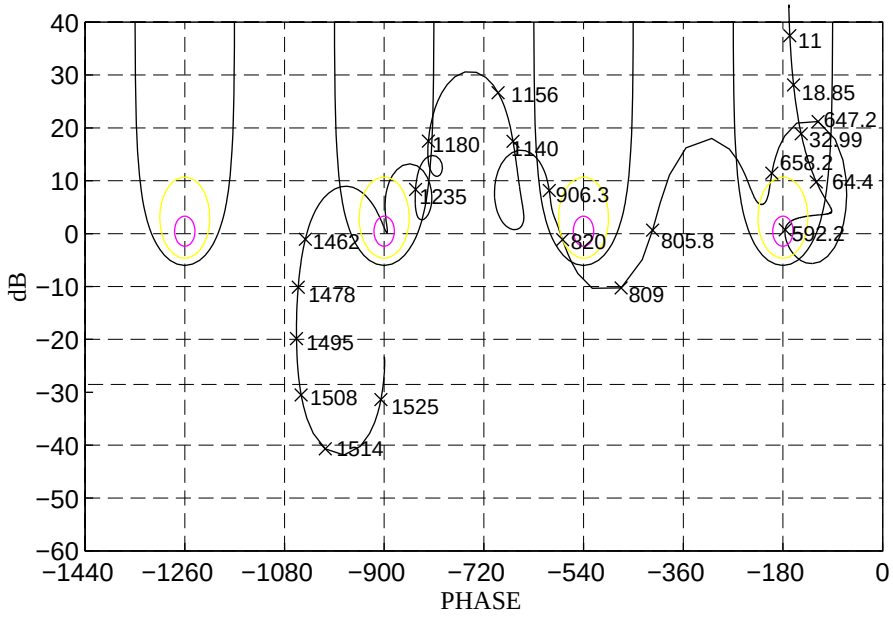

Figure 8: Rigid control - open loop Nichols plot (elevation axis)

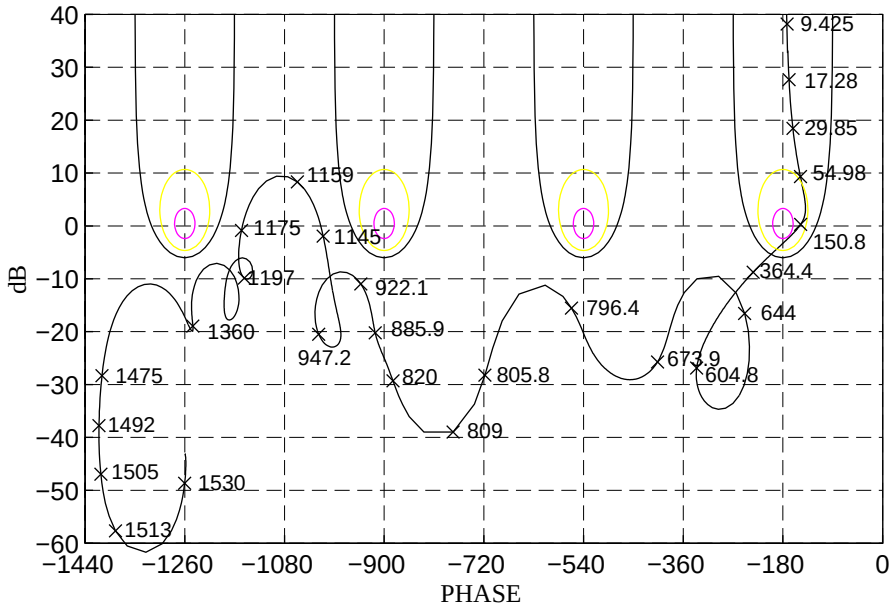

Figure 9: Classical approach - open loop Nichols plot (elevation axis)

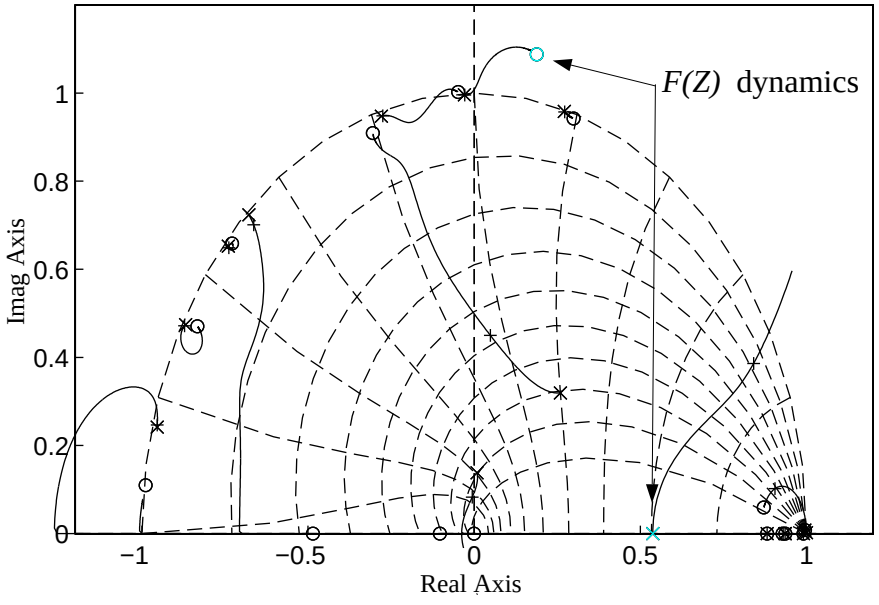

Figure 10: Classical approach - root locus (elevation axis)

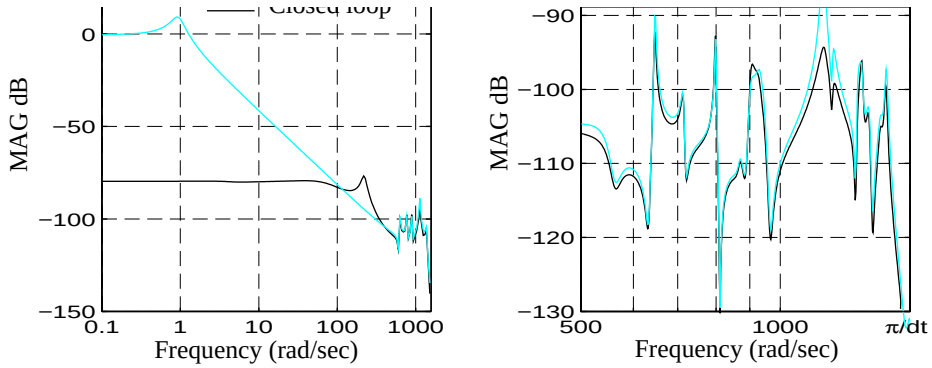

Figure 11: Classical approach - predicted elevation rejection function

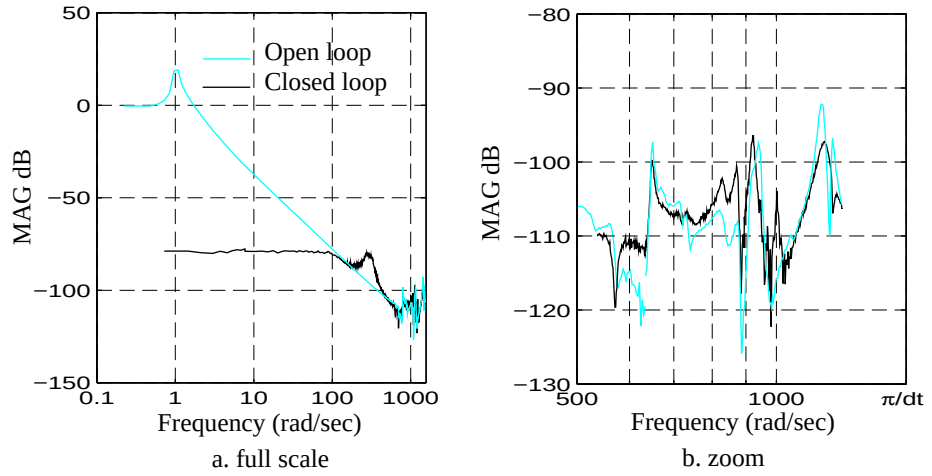

Figure 12: Classical approach - experimental elevation rejection function

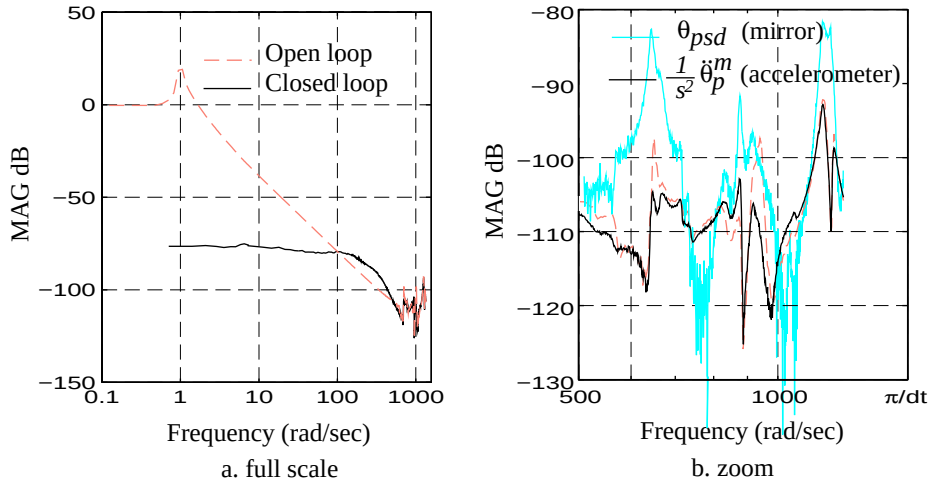

Figure 13: Robust H_2 synthesis - experimental rejection function

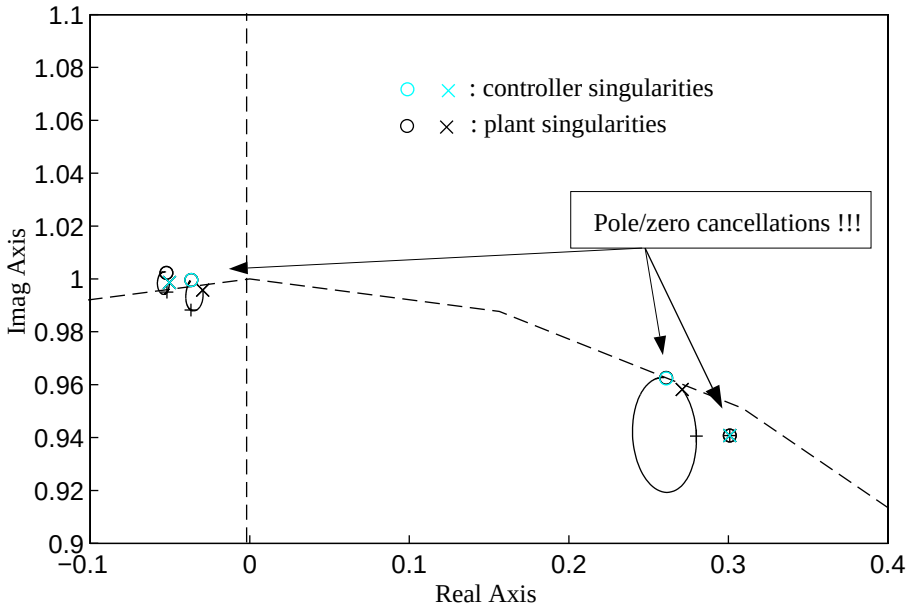

Figure 14: Performance H_2 synthesis - zoom on root locus with 6th order inertia model (elevation axis)

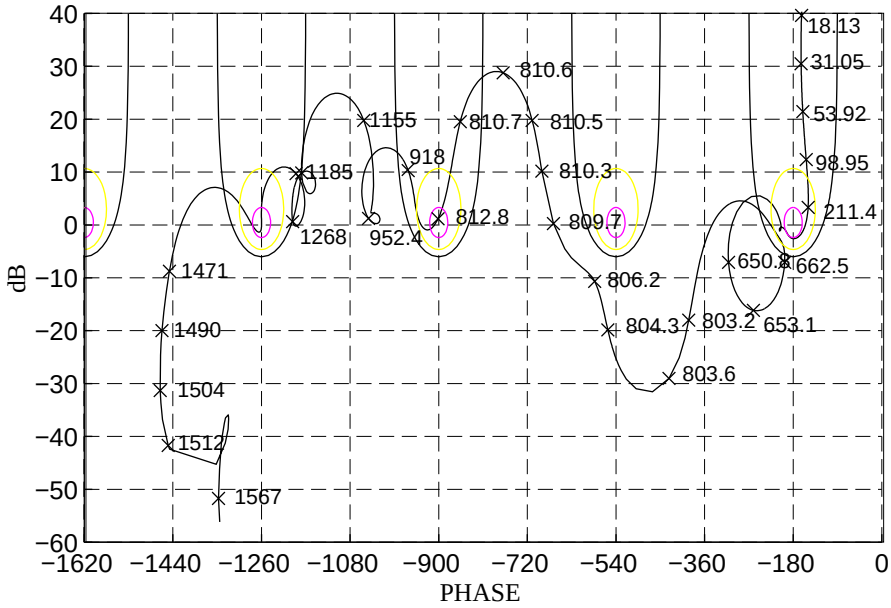

Figure 15: Performance H_2 synthesis - open loop Nichols plot with 14th order inertia model (elevation axis)

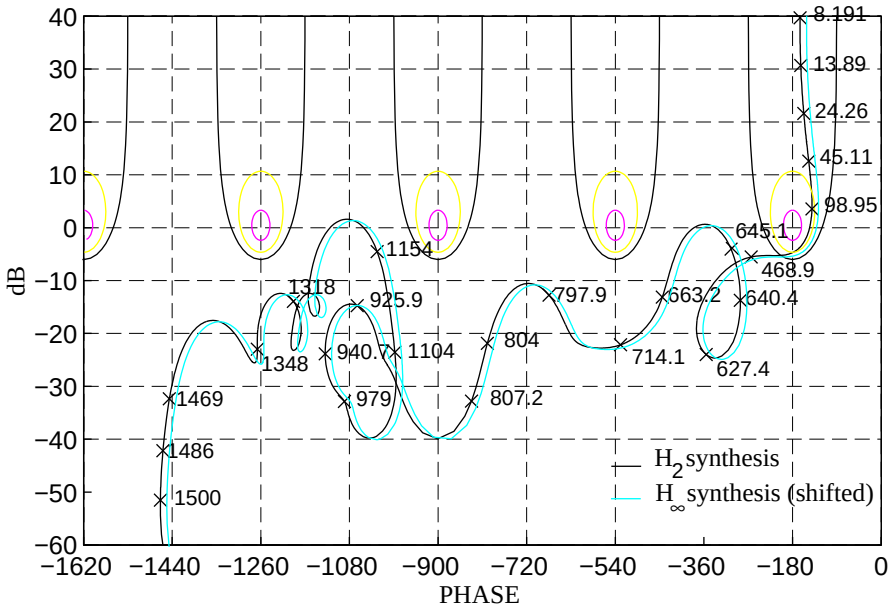

Figure 16: Robust synthesis - open loop Nichols plot with 14th order inertia model (elevation axis)

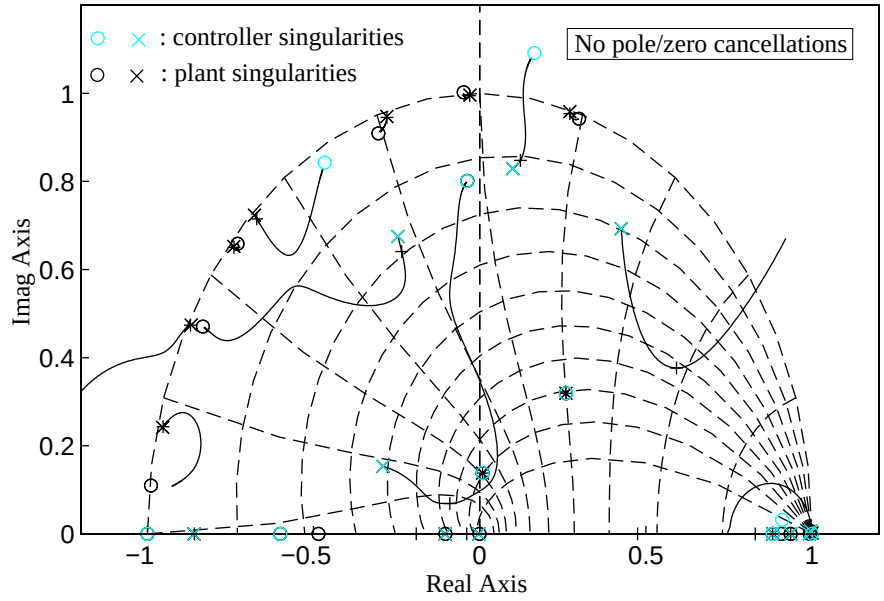

Figure 17: Robust synthesis - root locus with 14th order inertia model (elevation axis)